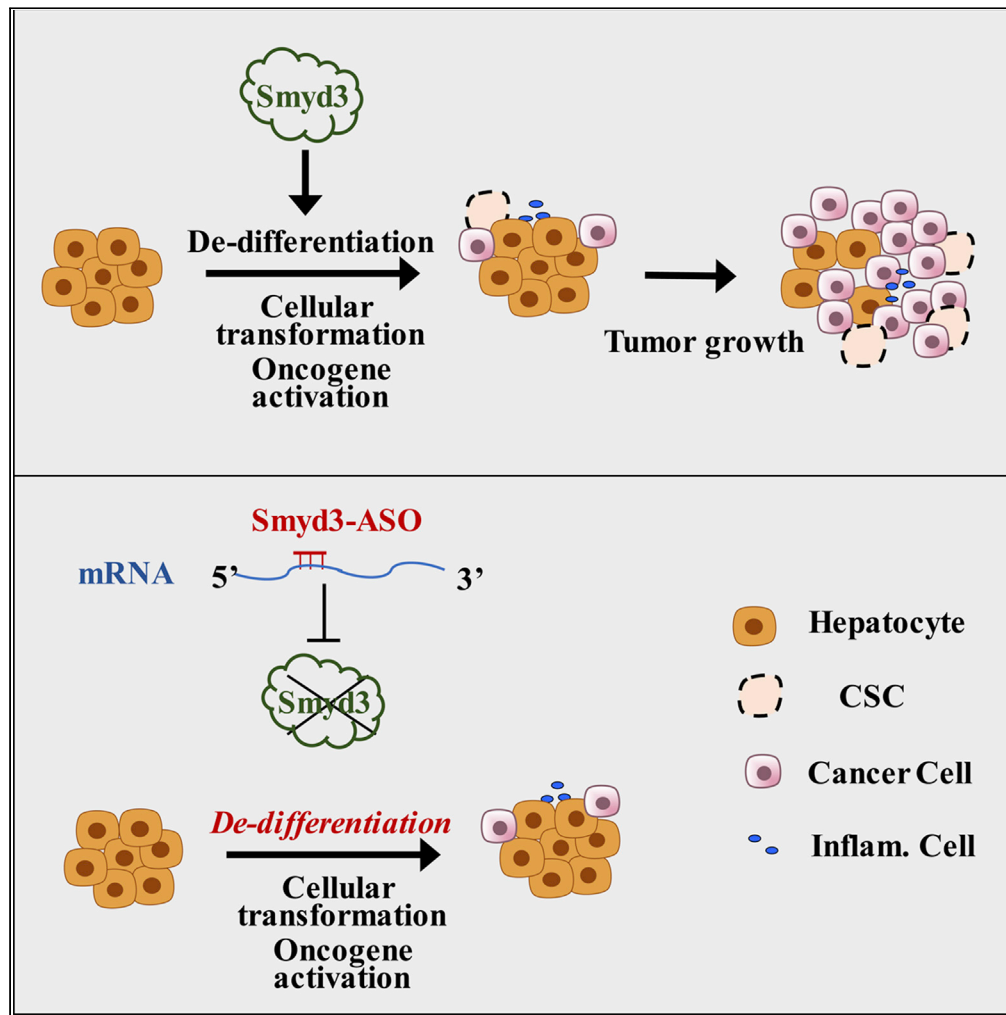## Article

Targeting Smyd3 by next-generation antisense oligonucleotides suppresses liver tumor growth

Haroula Kontaki, Marina Koukaki, Maria Vasilarou, ..., Xiaolin Luo, Youngsoo Kim, Iannis Talianidis

ysksilkroad@gmail.com (Y.K.)
talianid@imbb.forth.gr (I.T.)

Highlights

New generation antisense oligonucleotides efficiently silence Smyd3 *in vivo*.

Smyd3-ASO treatment inhibits the growth of already initiated liver tumors.

Smyd3-ASO treatment prevents the activation of oncofetal and CSC-specific genes.

Smyd3-ASO-sensitive gene signature specifies a de-differentiated phenotype.

iScience

Article

Targeting Smyd3 by next-generation antisense oligonucleotides suppresses liver tumor growth

Haroula Kontaki,[1,5] Marina Koukaki,[1,5] Maria Vasilarou,[1,4,5] Antonis Giakountis,[2,5] Elena Deligianni,[1] Xiaolin Luo,[3] Youngsoo Kim,[3,*] and Iannis Talianidis[1,6,*]

SUMMARY

The oncogenic function of suppressor of variegation, enhancer of zeste and MYeloid-Nervy-DEAF1-domain family methyltransferase Smyd3 has been implicated in various malignancies, including hepatocellular carcinoma (HCC). Here, we show that targeting Smyd3 by next-generation antisense oligonucleotides (Smyd3-ASO) is an efficient approach to modulate its mRNA levels *in vivo* and to halt the growth of already initiated liver tumors. Smyd3-ASO treatment dramatically decreased tumor burden in a mouse model of chemically induced HCC and negatively affected the growth rates, migration, oncosphere formation, and xenograft growth capacity of a panel of human hepatic cancer cell lines. Smyd3-ASOs prevented the activation of oncofetal genes and the development of cancer-specific gene expression program. The results point to a mechanism by which Smyd3-ASO treatment blocks cellular de-differentiation, a hallmark feature of HCC development, and, as a result, it inhibits the expansion of hepatic cancer stem cells, a population that has been presumed to resist chemotherapy.

INTRODUCTION

Genetic and epigenetic changes during carcinogenesis trigger de-regulated gene expression patterns, which in turn result in heterogeneous cellular phenotypes featuring uncontrolled cell proliferation, loss of cell-cell contacts, cellular invasiveness, and altered metabolic functions. Due to the high heterogeneity of the cells within tumor tissues and the sensitivity of normal cells to most cytotoxic agents, selective pharmacologic targeting of most cancer types is a formidable task. The repertoire of efficient treatment options may be substantially increased if specific drug targets which function selectively in cancer cells in a homogeneous manner are identified.

Our recent study suggested that Smyd3 may be a promising therapeutic target for the "difficult-to-treat" primary hepatocellular carcinoma (HCC), as it fulfills the requirements of cancer selectivity and functionality (Sarris et al., 2016). Smyd3 protein was hardly detectable in the normal liver while its expression was highly elevated in experimentally induced liver cancer. Importantly, using a Smyd3-KO mouse model, we have demonstrated that Smyd3 expression was required for the development of HCC (Sarris et al., 2016).

Smyd3 function has also been implicated in other types of cancer including colorectal cancer (Sarris et al., 2016; Giakountis et al., 2017), pancreatic ductal adenocarcinoma and adenovirus-induced lung adenocarcinoma (Mazur et al., 2014), and breast cancer (Fenizia et al., 2019; Hamamoto et al., 2006; Sarris et al., 2014). Mechanistic studies suggested that Smyd3 may exert its oncogenic activity via chromatin modifications, e.g., methylation of histone 3 lysine 4 (H3K4) or histone 4 lysine 5 (Giakountis et al., 2017; Hamamoto et al., 2004; Van Aller et al., 2012; Peserico et al., 2015). Nonetheless, in pancreatic and lung cancer cells, the main enzymatic target of Smyd3 is the cytoplasmic protein kinase MAP3K2 (Mazur et al., 2014). Methylation blocks MAP3K2 interaction with the PP2A phosphatase leading to de-repression of MAPK2 kinase activity, which in turn intensifies signaling from K-Ras to Erk1/2 (Mazur et al., 2014). In the liver, Smyd3 acts in the nucleus, where it invades transcriptionally active genomic regions via interactions with H3K4Me$_3$-modified histone tails and with RNA polymerase-II. In HCC, Smyd3 potentiates the expression of a variety of cancer-related genes, including several oncogenes and genes involved in cell proliferation or epithelial mesenchymal transition (Sarris et al., 2016).

[1]Institute of Molecular Biology and Biotechnology, FORTH, 70013 Herakleion, Crete, Greece

[2]Department of Biochemistry and Biotechnology, University of Thessaly, Larissa 41500, Greece

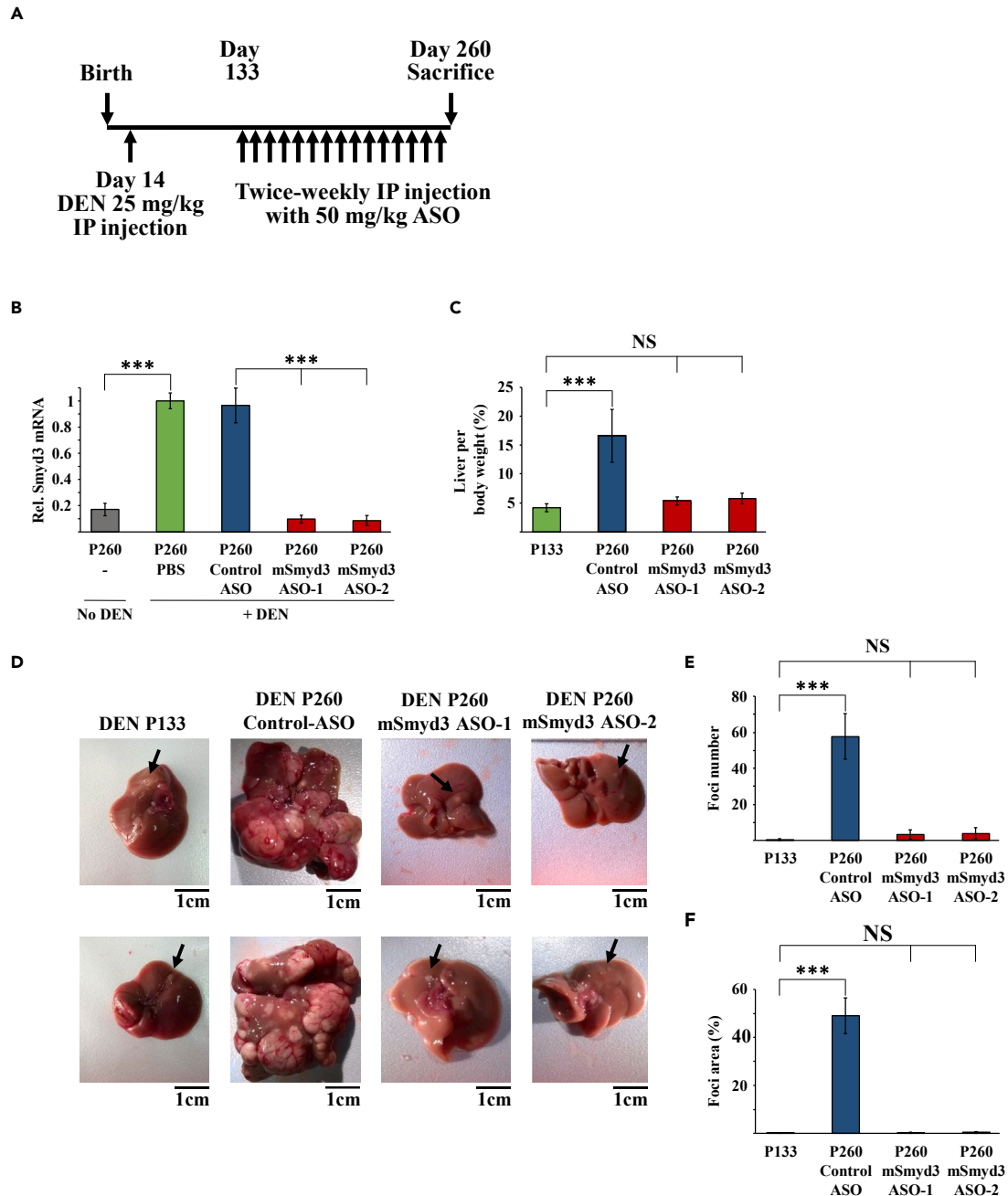[3]Ionis Pharmaceuticals, Carlsbad, CA, USA

[4]Department of Biology, University of Crete, 70013 Herakleion, Crete, Greece

[5]These authors contributed equally

[6]Lead contact

*Correspondence: ysksilkroad@gmail.com (Y.K.), talianid@imbb.forth.gr (I.T.)

Figure 1. Smyd3-ASO treatment attenuates tumor growth in DEN-induced liver cancer

(A) Schedule of treatments with 1,2-diethylnitrosamine (DEN) and antisense oligonucleotides.

(B) Relative Smyd3 mRNA levels in the livers of untreated (no DEN) or DEN-treated mice that received PBS injection once at P133 and sacrificed at P260 (P260 PBS) or treated with control-ASO or mSmyd3-ASO-1 or mSmyd3-ASO-2 from P133 according to the schedule indicated in (A). Bars represent average Smyd3 mRNA levels normalized to Gapdh mRNA and SEM from 5 individual mice.

(C) Liver per body weight ratios in DEN and control-ASO or mSmyd3-ASO-1 and mSmyd3-ASO-2-treated mouse livers. Bars represent mean values and SEM from 4 DEN-treated mice at P133, from DEN-induced mice at P260 that were treated with mSmyd3-ASO-1 (n = 9) or mSmyd3-ASO-2 (n = 9), and DEN-induced mice at P260 treated with control-ASO (n = 9).

(D) Macroscopic appearance of two representative livers from DEN-treated mice at day 133 after birth (P133) (n = 4) and DEN-treated mice at day 260 after birth (P260) that were treated either by control-ASO (n = 9) or mSmyd3-ASO-1 (n = 9) or mSmyd3-ASO-2 (n = 9) twice weekly following day 133. Arrows indicate small tumor foci.

Figure 1. *Continued*

(E and F) Average number of visible tumor foci (E) and the proportion of the surface (F) of the livers covered by tumor foci at the different conditions. Bars represent mean values and SEM from 4 DEN-treated mice at P133, from DEN-induced mice at P260 that were treated with mSmyd3-ASO-1 (n = 9) or mSmyd3-ASO-2 (n = 9), and DEN-induced mice at P260 treated with control-ASO (n = 9).

See also Figure S1.

Studies on Smyd3-KO mice were instrumental in deciphering the molecular mechanisms responsible for the oncogenic function of Smyd3 in different cancer types. They also established the view that Smyd3 is a promising drug target. Although the genetic models lack Smyd3 from the time of conception, which limit their value for pharmacological studies, analyses of knockout mice provided clues for the potential strategy of targeting Smyd3 in different cancer types. For example, in liver or breast cancer, where the methylase activity of Smyd3 is dispensable for the potentiation of expression of cancer-related genes (Sarris et al., 2016; Fenizia et al., 2019), the use of enzymatic inhibitors is not a preferred targeting scheme as opposed to pancreatic and lung cancer, where Smyd3 acts mainly through methylation of MAPK2 (Mazur et al., 2014). Hence, in order to target Smyd3 function in liver cancer, we sought for means influencing Smyd3 expression levels.

Antisense oligonucleotide (ASO)-mediated mRNA silencing has been demonstrated as a safe and highly specific targeting approach, alternative to the use of enzymatic inhibitors or neutralizing antibodies (Kole et al., 2012). ASOs hybridize to the target mRNAs and activate RNAse H, which cleaves the RNA moiety of the heteroduplex (Kole et al., 2012). ASOs synthesized by next-generation chemistry have increased binding affinity, nuclease resistance, and enhanced biostability (Seth et al., 2009; Murray et al., 2012). The efficacy of ASO-based therapy in clinics has already been demonstrated in several cases, including neurodegenerative diseases, metabolic syndrome, and cancer (Linnane et al., 2019; Hong et al., 2015; De Velasco et al., 2019; Xiao et al., 2018; Xu et al., 2019; Kim et al., 2019a, 2019b; Arun et al., 2016).

Taking into consideration the above, we explored a novel ASO-based strategy to target Smyd3 in mouse models of HCC and human liver cancer-derived cell lines.

RESULTS

Smyd3-ASO treatment decreases tumor burden in a mouse model for hepatocellular carcinoma

To investigate whether pharmacological inhibition of Smyd3 may influence HCC progression, we have injected diethylnitrosamine (DEN)-treated C57Bl/6J mice with Smyd3-ASOs. In this standard chemically induced carcinogenesis model, mice receive a single injection of DEN at postnatal day 14 and visible liver tumors develop around the eighth month of age (Maeda et al., 2005). The hepatotoxic agent at early life initiates a complex inflammation-dependent tumorigenesis process, which is destined to culminate to HCC with tumor penetrance nearly at 100% (Sarris et al., 2016; Maeda et al., 2005). The different Smyd3-ASOs used in the study were selected based on their benign properties in a 4-week rodent tolerability study (100 mg/kg/week), where they displayed no notable effects on organ weights, serum alanine aminotransferase (ALT), aspartate aminotransferase, bilirubin, urea nitrogen, and albumin levels compared to treatments with phosphate buffered saline (PBS) (Figures S1A–S1D).

DEN-induced mice received twice weekly mSmyd3-ASOs or control-ASO by intraperitoneal injection from postnatal day 133 (P133) and were sacrificed for analyses at day 260 (P260) (Figure 1A). Normal and DEN-induced levels of hepatic Smyd3 mRNA were reduced in mSmyd3-ASO-treated mice at 4 weeks or P260, respectively, while there was little difference between PBS-treated and control-ASO groups (Figures 1B and S1F). DEN-mediated liver weight increase was also prevented by mSmyd3-ASO treatment (Figure 1C). We note that similar effects were detected by treatments with mSmyd3-ASO-1 and mSmyd3-ASO-2, which target different regions of Smyd3 mRNA. Furthermore, both mSmyd3-ASOs efficiently silenced Smyd3 mRNA expression in the livers and colons of a different mouse strain, BALB/c, following 4-week treatments (Figure S1E). This demonstrates the efficiency and specificity of ASO-mediated silencing of Smyd3.

Macroscopic evaluation of livers from DEN-treated P260 mice revealed that mSmyd3-ASO treatment had a dramatic effect on liver tumor development. At day 133 (P133), when ASO treatment started, macroscopically visible tumorous foci could scarcely be observed, suggesting that tumorigenesis is still at an early phase (Figures 1D–1F). At P260, however, control-ASO-treated mice developed full-blown HCC with

A

B
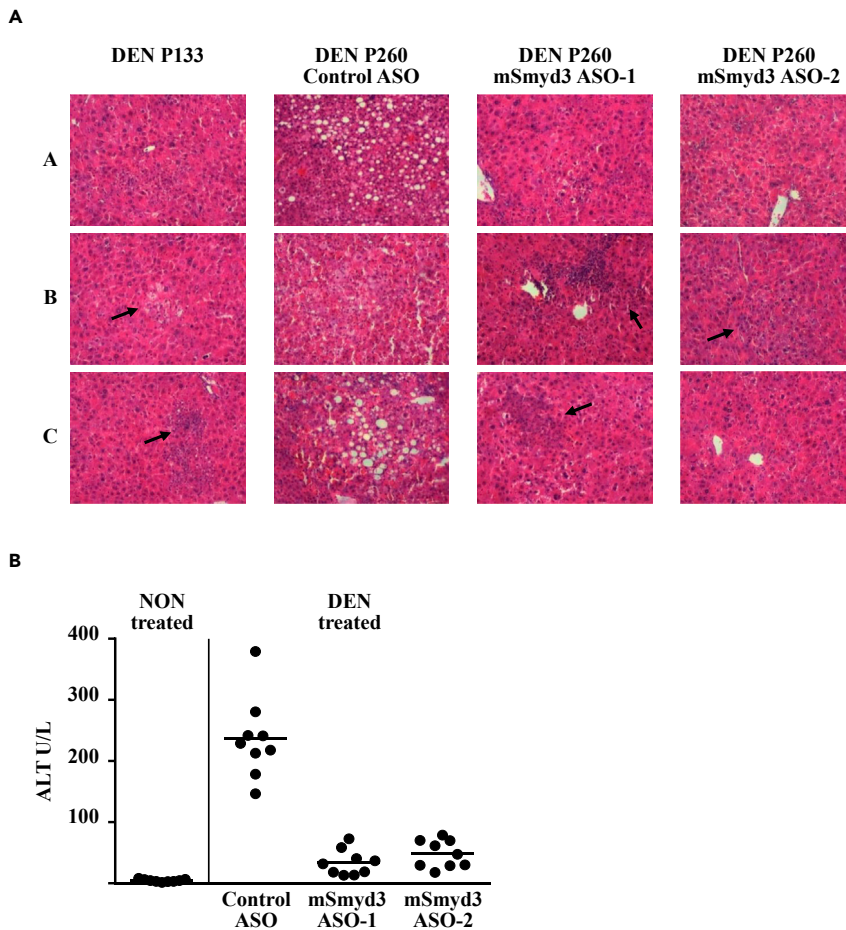
Figure 2. Modest histopathological lesions and reduced serum ALT levels in DEN-induced mice following Smyd3-ASO treatment

(A) Three (A, B, and C) representative fields of H&E-stained liver sections in DEN-treated mice at P133 and at P260 following treatments with control-ASO or mSmyd3-ASOs as in Figure 1. Arrows indicate dysplastic or hyperplastic nodules.
(B) Serum alanine aminotransferase (ALT) levels in untreated normal mice and in DEN-treated mice at P260. DEN-treated mice received two different mSmyd3-ASOs or control-ASO twice weekly following day 133 (n = 9).
See also Figure S2.

several large and small foci covering the entire organ. Only very few and small foci were visible in the livers of mSmyd3-ASO-treated P260 mice, which resembled more the P133 livers (Figures 1D–1F). Importantly, the two Smyd3 ASOs with similar potency were very similar in eliciting phenotypic changes, suggesting target-mediated specific effects.

The livers of P260 control-ASO-treated mice, as expected, displayed several classical histological features of HCC including nuclear atypia, increased eosinophilic inclusions, cytoplasmic clearance, irregular trabeculae, obliterated portal tracts, and frequent mitotic figures (Figure 2A). In sharp contrast to this, we could observe only few nodular hyperplastic areas and only a very small number of cells with cytoplasmic clearance or eosinophilic inclusions in the liver sections of both P260 mice groups treated with mSmyd3-ASOs (Figure 2A). The overall histological profile of P260 Smyd3-ASO-treated mice highly resembled that of P133 mice, suggesting that mSmyd3-ASO treatment results in a highly reduced tumor burden, probably by preventing the expansion of early-developed small cancer foci into larger tumor masses.

The above differences in the frequency of histologically defined tumorous regions were confirmed by immune-histochemical staining for the proliferation marker Ki-67. The number of Ki-67 positive cells ranged

Figure 3. Smyd3-ASO treatment alters cancer-specific transcriptome in DEN-induced mouse liver cancer

(A) Principal component analysis (PCA) plots of the global mRNA expression patterns in untreated P260 normal mice (purple dots, n = 5), in DEN-treated mice at P133 (green dots, n = 4), and in DEN-treated mice at P260 that were treated additionally either by control-ASO (blue dots, n = 6) or mSmyd3-ASO-1 (red dots, n = 6) twice weekly following day 133. The percentage of variance explained by each principal coordinate is indicated.

(B) Hierarchical clustering analysis and the corresponding heatmap of differentially expressed genes. Each column shows differentially expressed genes in the livers of DEN-treated mice at P260 and P133, relative to those in the livers of untreated P260 and P133 mice. Only differentially expressed genes were included in the heatmap. The conditions indicated are as described in (A). The color scale bar indicates the range of fold changes relative to samples from untreated mice. Representative genes whose differential expression has been validated by RT-PCR are indicated at right: green fonts,

Figure 3. *Continued*
mSmyd3-ASO-1-sensitive, DEN-downregulated genes; black fonts, Smyd3-ASO-1-sensitive, DEN-upregulated genes; red fonts, Smyd3-ASO-1-sensitive, DEN-upregulated cancer stem cell signature genes.
(C) Venn diagrams depicting the fractions of mSmyd3-ASO-1-sensitive genes in DEN-upregulated and DEN-downregulated gene sets.
(D) Ranked coverage plot of the expression changes of "oncofetal" genes in control-ASO (blue dots, n = 6) or mSmyd3-ASO-1 (red dots, n = 6) treated mice.
(E) High scoring pathways and hallmark gene sets identified by Gene Set Enrichment Analysis (GSEA) of mSmyd3-ASO-sensitive genes. Normalized enrichment scores (NES) and statistical parameter false discovery rate (FDR) q-values are shown. Note the orders of magnitude difference of FDR q-values between DEN-downregulated gene sets compared to DEN-upregulated gene sets.
See also Figure S3.

from 33 to 62 per high power field in liver sections from control-ASO-treated mice as opposed to the 0 to 4 positive cells in those treated with mSmyd3-ASO (Figures S2A and S2B).

In agreement with the macroscopic and histological data, we found that mSmyd3-ASO treatment prevented the dramatic increase of serum ALT levels in DEN-treated mice, an indicator of HCC-associated liver dysfunction (Figure 2B).

Taken together, the above results demonstrate that silencing of Smyd3 by mSmyd3-ASOs at a stage when experimentally induced liver carcinogenesis has already been initiated significantly attenuates further progression of the tumors. Although small cancer foci are still detectable, the overall tumor burden is drastically reduced in mSmyd3-ASO-treated mice.

Smyd3-ASO treatment impedes the development of liver cancer-specific gene expression patterns in mice

To evaluate potential mSmyd3-ASO treatment-mediated changes in global gene expression patterns, we performed RNA sequencing (RNA-seq) analyses from DEN-treated P260 mice, which received control-ASO or mSmyd3-ASO-1 or mSmyd3-ASO-2 and compared to those of DEN-treated P133 or untreated P260 (no DEN injection) mice. Principal component analysis (PCA) of the data revealed significant variations between the expression patterns in the above conditions (Figure 3A). As expected, the data sets from the liver tumors of control-ASO-treated mice greatly varied from those of normal (non-cancerous) or P133 (early stage cancer) mice. Interestingly, the expression pattern in the livers of mSmyd3-ASO-1-treated mice also greatly varied from all other samples. The divergence between the expression profiles of mSmyd3-ASO-treated and P133 livers suggests that despite the similar phenotypic appearance, these livers have a cellular composition with different molecular phenotypes. Notwithstanding, the high degree of variation between mSmyd3-ASO and control-ASO-treated mice pointed to the possibility that key features of the cancer-specific gene expression program are not developed following mSmyd3-ASO administration. Comparison of the gene expression patterns in the livers of mSmyd3-ASO-1 and mSmyd3-ASO-2-treated mice revealed nearly perfect (r = 0.995) match (Figure S3A). Since the two ASOs target different regions of the Smyd3 mRNA, the latter result largely eliminates the possibility of potential "off-target" effects.

Hierarchical clustering analysis of the differentially expressed genes identified large clusters of genes whose expression greatly varied between P133, P260 mSmyd3-ASO-1-treated, and control-ASO-treated livers (Figure 3B). Some, but not all, of the differences between P133 and control-ASO-treated samples could be detected in mSmyd3-ASO-1-treated samples (Figure 3B).

Next, we retrieved the list of genes whose expression changes were sensitive to ASO treatment. Using a cutoff of 1.5-fold change and false discovery rate <0.05, we identified 1019 upregulated and 717 downregulated genes in DEN-induced tumors (Figure 3C). Among the 1019 DEN-induced genes, activation of 537 was prevented by mSmyd3-ASO treatment, while among the 717 DEN-silenced genes, mSmyd3-ASO-1 treatment prevented the repression of 219 genes (Figure 3C).

Key constituents of this "mSmyd3-ASO-1-sensitive DEN-induced" gene list are the 33 "oncofetal" genes like Afp, H19, Prom1/2, Gpc3, Plk1, Igf2, Dlk1 (Figure 3D), and a number of genes highly expressed in cancer cells with "stemness" features, like Sox9, Sox4, Gpc3, Aldh1b1, Prom1/2, Arid4a, Dusp1, Sall1, Snai2, Dntt, Spp1, Tff3, Esm (Figure 3B). The term "oncofetal genes" is used for the genes that are highly expressed in the embryonic liver, fully silenced following birth and reactivated in HCC (Nikolaou et al., 2015; Karagianni et al., 2020). Re-expression of these genes in cancer denotes the loss of tight regulation

of gene expression during carcinogenesis, which drives de-differentiation. The lack of upregulation of the majority of the studied oncofetal genes suggests that Smyd3-ASO treatment impaired the process of carcinogenesis at a stage prior to the induction of cellular de-differentiation events.

Further evidence for the prevention of cancer-dependent de-differentiation process by mSmyd3-ASO-1 treatment was provided by Gene Set Enrichment Analysis of the Smyd3-ASO-sensitive genes. As shown in Figures 3E and S3B, mSmyd3-ASO-1-sensitive DEN-induced genes were enriched in categories of cancer- and growth-related pathways and embryonic stem cell-related biological processes. On the opposite side, mSmyd3-ASO-1-sensitive DEN-repressed genes were mostly enriched in metabolism-related gene set categories, which are characteristic to differentiated hepatocyte phenotype (Figures 3E and S3B). Importantly, the enrichment values of the latter pathways had consistently better significance scores compared to those obtained by the DEN-induced gene set.

Correlation between the expression of differentiation-specific Smyd3-ASO-sensitive genes and clinical parameters of patients with HCC

To assess the relevance of the mSmyd3-ASO-1-sensitive gene signatures in human HCC, we have interrogated the data from 341 HCC subjects available in The Human Cancer Genome Atlas (TCGA) (Cancer Genome Atlas Network et al., 2017). We first ranked the data sets from 341 HCC and 46 paracancerous biopsies to assess tumorigenicity features via PCA projection (Figure 4A). Subsequently, we determined the corresponding ranks of the 537 mSmyd3-ASO-1-sensitive tumor-dependent upregulated and 219 Smyd3-ASO-sensitive tumor-dependent downregulated genes, as well as the 33 mSmyd3-ASO-1-sensitive oncofetal genes. As shown in Figure 4B, mSmyd3-ASO-1-sensitive upregulated genes are distributed in median ranks, suggesting that as an entire group, they do not significantly contribute to tumorigenic features of human HCC. On the other hand, the "oncofetal" subset of the mSmyd3-ASO-1-sensitive upregulated genes is ranked low (closer to 1), supporting the conclusions of our pathway analyses that Smyd3-ASOs influence genes involved in cancer-specific de-differentiation processes. In agreement with this, mSmyd3-ASO-1-sensitive tumor-dependent downregulated genes ranked high (close to 20.000 position), a distribution corresponding to genes negatively correlating with tumorigenicity. Such distribution is characteristic to tumor suppressors and gene expression signatures of highly differentiated hepatocytes.

The rank distribution of the mSmyd3-ASO-1-sensitive gene sets did not indicate significant correlations with the probability of overall survival (OS) rates of the patients (Figure 4C). Since OS is a complex feature, which is influenced by several factors, we further analyzed the effects of each mSmyd3-ASO-1-sensitive genes within the "upregulated" and "downregulated" groups by scoring them "high" or "low", if their higher or lower expression corresponded to significant shortening of survival time, while gene effects without statistical significance were scored "none". Among the 537 mSmyd3-ASO-1-sensitive tumor-dependent upregulated genes, the percent of genes with high and low score was similar (27.2 and 32.6, respectively), while the others were in the category with no statistical significance (40.2%) (Figure 4D). The net effect should be of low impact on OS, which essentially recapitulates the results of the survival rank analysis. In contrast to this, among the 219 mSmyd3-ASO-1-sensitive downregulated genes, the ones with "low" score (57.4%) significantly outnumbered the genes with "high" (8.1) or non-significant (34.6) scores, suggesting that the lack of downregulation of a significant portion of these genes would have a net effect of increasing the OS probability of patients with HCC (Figure 4D).

Analysis of the effects of the mSmyd3-ASO-1-sensitive gene signatures on the clinical parameters of tumor grade or tumor stage progression revealed that, similar to the "tumorigenicity" profiles, mSmyd3-ASO-1-sensitive tumor-dependent downregulated genes ranked high in both of these probability plots, demonstrating a strong negative correlation between the expression of these genes with tumor grade and tumor stage progression (Figures 4E and 4F). Plotting the ranks of the entire group of Smyd3-ASO-sensitive tumor-dependent upregulated genes did not reveal significant correlations, but the distribution of the "oncofetal" subset of this group was clearly shifted toward low ranks, indicating their strong association with both tumor grade and tumor stage progression (Figures 4E and 4F).

Taken together, the above analyses suggest that, in human HCC, the expression of mSmyd3-1-ASO-sensitive genes, which are responsible for the de-differentiated phenotype of tumors, correlates with tumorigenicity and important clinical parameters like OS, tumor stage, and tumor grade progression.
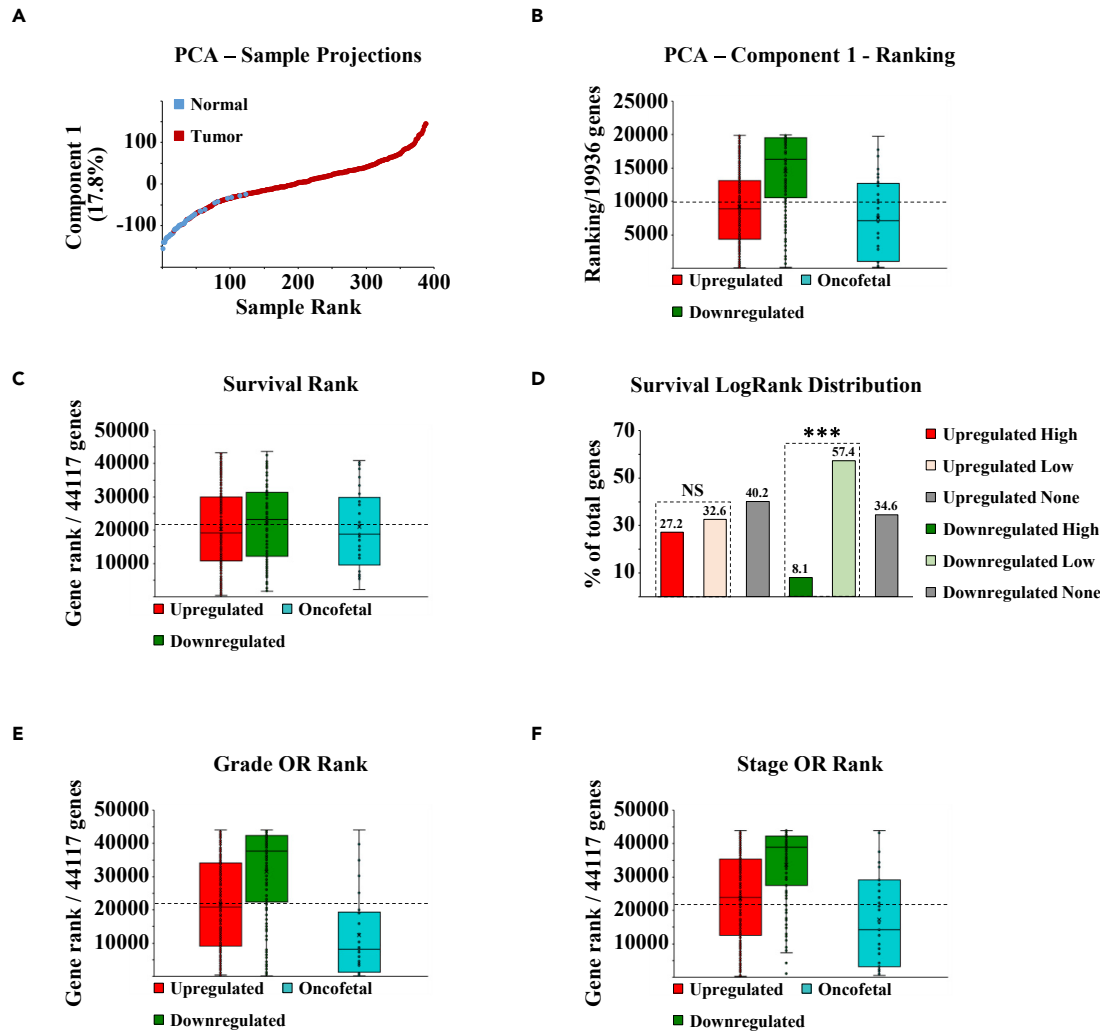
Figure 4. Effects of Smyd3-ASO-sensitive genes on tumorigenicity, the probability of overall survival, tumor stage, and tumor grade progression in human HCC

(A) Principal component analysis (PCA) projection of ranked liver hepatocellular carcinoma samples from TCGA database. Negative PC1 values (blue dots) associate with normal samples, while positive values (red dots) associate with tumor samples.

(B) Gene ranking distribution plots of mSmyd3-ASO-1-sensitive DEN-upregulated (red bars) or DEN-downregulated (green bars) or oncofetal (blue bars) genes based on PCA component 1 score. Low ranks (close to zero) associate with positive PC1 values, indicating oncogenic features, while high ranks (close to 20.000) associate with negative PC1 values, indicating oncosuppressor features.

(C) Gene ranking distribution plots of Smyd3-ASO-sensitive gene sets based on odds ratios of overall survival (color codes as in [b]). Ranking was based on odds ratio for each expressed gene (total genes: 44,117). High ranking indicates that high gene expression increases the odds of surviving (gene behaves as a tumor suppressor).

(D) Overall survival effect distribution of mSmyd3-ASO-1-sensitive gene sets. Bars show the percentage of mSmyd3-ASO-1-sensitive genes whose high-level expression ("high") or whose low-level expression ("low") reduces survival time. "High" indicates that high gene expression (above gene median for all patients) reduces survival time (oncogene effect), and "low" indicates that low gene expression (below gene median for all patients) reduces survival time (oncosuppressor effect). The percentage of genes whose differential expression has no effects on survival is depicted as ("none").

(E and F) Gene ranking distribution plots of mSmyd3-ASO-1-sensitive genes based on odds ratio for tumor grade (E) and for tumor stage (F). Ranking was based on odds ratio for each expressed gene (total genes: 44,117). High ranking (close to 44,117) indicates that high gene expression decreases the odds of progressed tumor stage or undifferentiated tumor stage (gene effect is tumor suppressing), while low ranking indicates OR>1 (close to zero), i.e., that high expression increases the odds of progressed tumor stage or undifferentiated tumor stage (gene effect is oncogenic).

See also Figure S4.

Since Smyd3-ASOs act via lowering Smyd3 mRNA levels, we asked whether the correlation of Smyd3-regulated ASO-sensitive genes with tumor grade and tumor stage is a direct consequence of lower Smyd3 mRNA levels in mSmyd3-ASO-1-treated mice. To this end, we analyzed the correlation of Smyd3 expression with tumor stage

and tumor grade using two independent approaches: Kaplan-Meier survival plot approach, which takes into account temporal parameters, and gene ranking approach according to ODD ratios for tumor stage and tumor grade features, which only gives an overall estimate of the correlation without considering time-dependent changes (Figures S4A and S4B). A significant correlation between Smyd3 mRNA levels and tumor grade was evident by both approaches, which supports our conclusions that Smyd3 regulates cellular de-differentiation and cancer stem cell (CSC) properties, since tumor grades describe cellular phenotypes of HCC related to the differentiation state of the cells. Using Edmonson-Steiner nuclear grading system, grade 1/2 corresponds to "well-differentiated" cellular phenotype, grade 3 corresponds to "moderately differentiated" phenotype, and grade 4 corresponds to "poorly differentiated" phenotype. On the other hand, the correlation between Smyd3 mRNA levels and overall probability of tumor stage progression was marginal but not statistically significant (Figures S4A and S4B). Tumor staging reflects the size, the number, and the metastatic spread of cancerous lesions in the body. The lack of statistically significant correlation suggests that Smyd3 effect on tumor stage needs time for activation of downstream effectors to become significant. Visual comparison of the Kaplan-Meier plots over time supports the above notion: In the beginning, the two curves overlap, but later, they become separated and the difference between them increases progressively.

Taken together, we conclude that Smyd3-mediated regulation of specific target genes can influence both closely related clinical features: tumor stage and tumor grade. The results highlight the importance of Smyd3 regulatory function on the observed phenotypes.

Silencing Smyd3 expression by Smyd3-ASOs alleviates CSC-related functions of human liver cancer-derived cell lines

To test whether Smyd3 silencing can influence the cancer phenotype of already established human HCC cells, we treated 6 different human HCC cell lines with hSmyd3-ASOs. To avoid potential non-specific effects on cell proliferation, treatments were via "free uptake" without using transfection agents, as described in our previous report (Hong et al., 2015). As shown in Figures S5 and S6, efficient inhibition of Smyd3 mRNA and protein levels could be detected in HLF, SNU398, SNU423, and SNU449 hepatic cell lines, with SNU398 being the most sensitive to hSmyd3-ASOs. HuH7 and SNU387 cells were relatively resistant to hSmyd3-ASO treatment. Such resistance is observed in some established cell lines, mainly due to poor cellular uptake (Linnane et al., 2019). We, therefore, used HuH7 or SNU387 cells as negative controls and did not further investigate the mechanism of resistance to free uptake.

As expected, hSmyd3-ASO treatment did not affect the growth rate of the resistant HuH7 or SNU387 cell lines (Figure 5A). On the other hand, significant growth retardation was detectable in the sensitive HLF, SNU398, SNU423, and SNU449 cells (Figure 5A).

To evaluate potential effects in the tumorigenic properties, we first evaluated the clonogenic growth and migration activity of the cells. Colony formation capacity was significantly reduced by hSmyd3-ASO treatment in the sensitive HLF, SNU398, and SNU423 cells but not in SNU449 cells (Figure 5B). Analyses of the migration capability by transwell assays revealed that hSmyd3-ASOs significantly reduced the migration potential of HLF and SNU449 cells but not that of SNU423 or SNU398 cells (Figure S7). We note that SNU398 cells have a low intrinsic migration potential.

Next, we performed anchorage-independent tumor spheroid cultivation assays to evaluate effects on self-renewal capacity of the CSC population in the hepatic cell lines. In these assays, cells are grown in serum-free, growth factor-supplemented media in non-adherent conditions under which only cancer stem/progenitor cells can survive and initiate the formation of solid 3D structures, called oncospheres or tumor spheres (Ward Rashidi et al., 2019; Pandit et al., 2018). Among the cell lines investigated, SNU449 did not form 3D sphere structures even after long time culturing periods (Figure S8). We observed high oncosphere formation capacity by the HuH7, HLF, SNU398, and SNU423 cells (Figure 6). hSmyd3-ASO treatment significantly reduced the number of oncospheres formed by the sensitive HLF, SNU398, and SNU423 cells but not by the insensitive HuH7 cells (Figure 6). These results suggest that hSmyd3-ASO treatment inhibits the "stemness" features of the subpopulation of HLF, SNU398, and SNU423 cells, which are required for the initiation and growth of 3D tumor-like structures *in vitro*.

The negative effect of hSmyd3-ASOs in the tumorigenic activity of the cells was further investigated by xenograft assays. Following subcutaneous injection of immunocompromised mice with HuH7, HLF, SNU398, SNU423, and
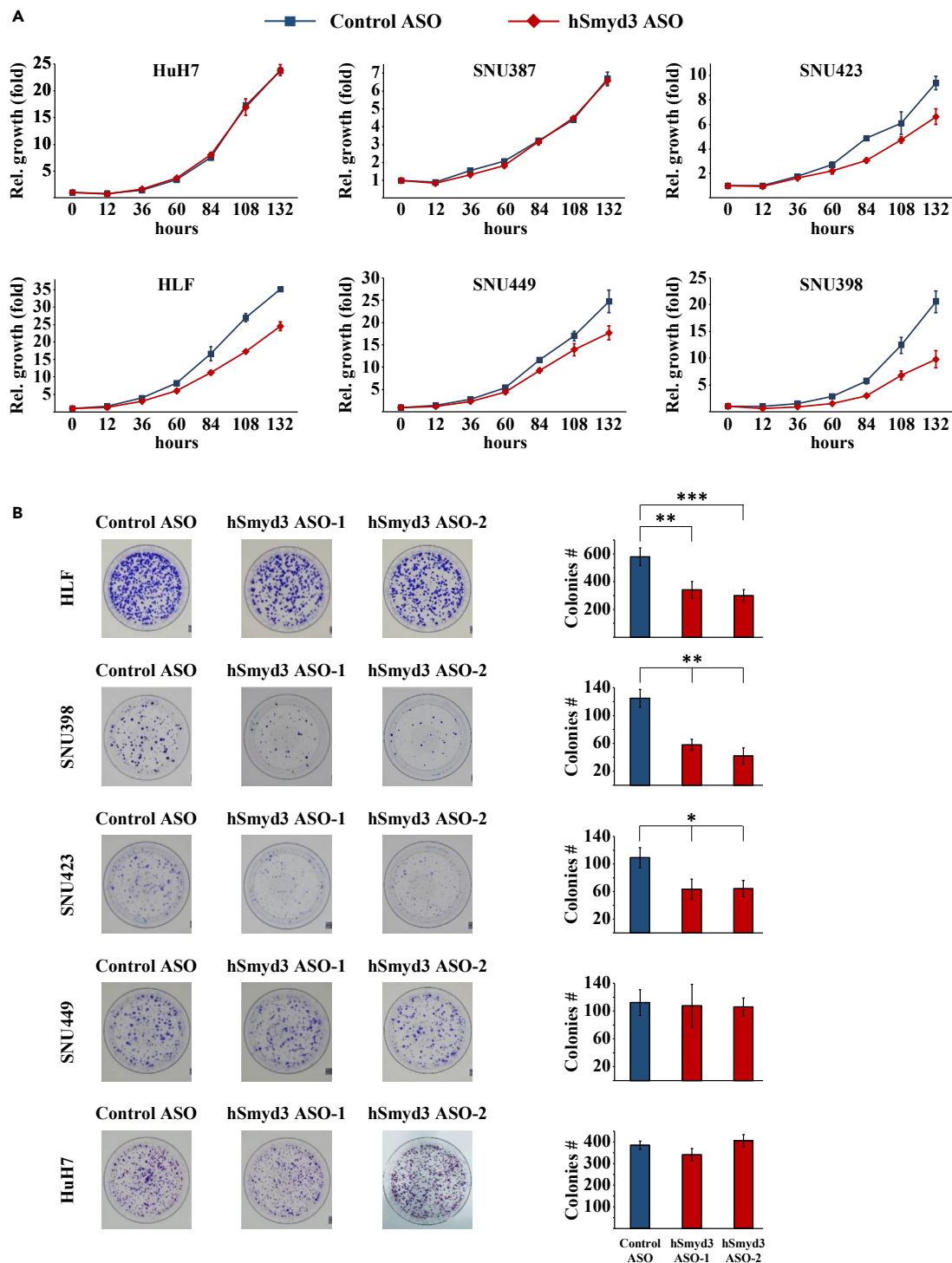
Figure 5. Smyd3-ASO treatment inhibits proliferation rates and colony formation ability of human hepatocellular carcinoma cell lines

(A) Growth curves of HuH7, SNU387, HLF, SNU398, SNU423, and SNU449 cell lines treated with 0.2 μM control-ASO (blue lines) or hSmyd3-ASO-1 (red lines). The cells were pretreated with the ASOs for one passage before plating. Data points represent mean values of the fold increase in cell numbers compared to time 0 (12 hr after seeding) and SEM from 3 independent experiments.

(B) Colony formation capacity of HLF, SNU398, SNU423, SNU449, and HuH7 cell lines treated with 0.2 μM control-ASO or hSmyd3-ASO-1 or hSmyd3-ASO-2. The cells were seeded at a density of 1000 cells per 100 mm plate and fixed after 18-22 days. ASO-containing medium was replaced every 3 days. Bars represent the average number of colonies per plate and SEM from 3 experiments.

See also Figures S5–S7.
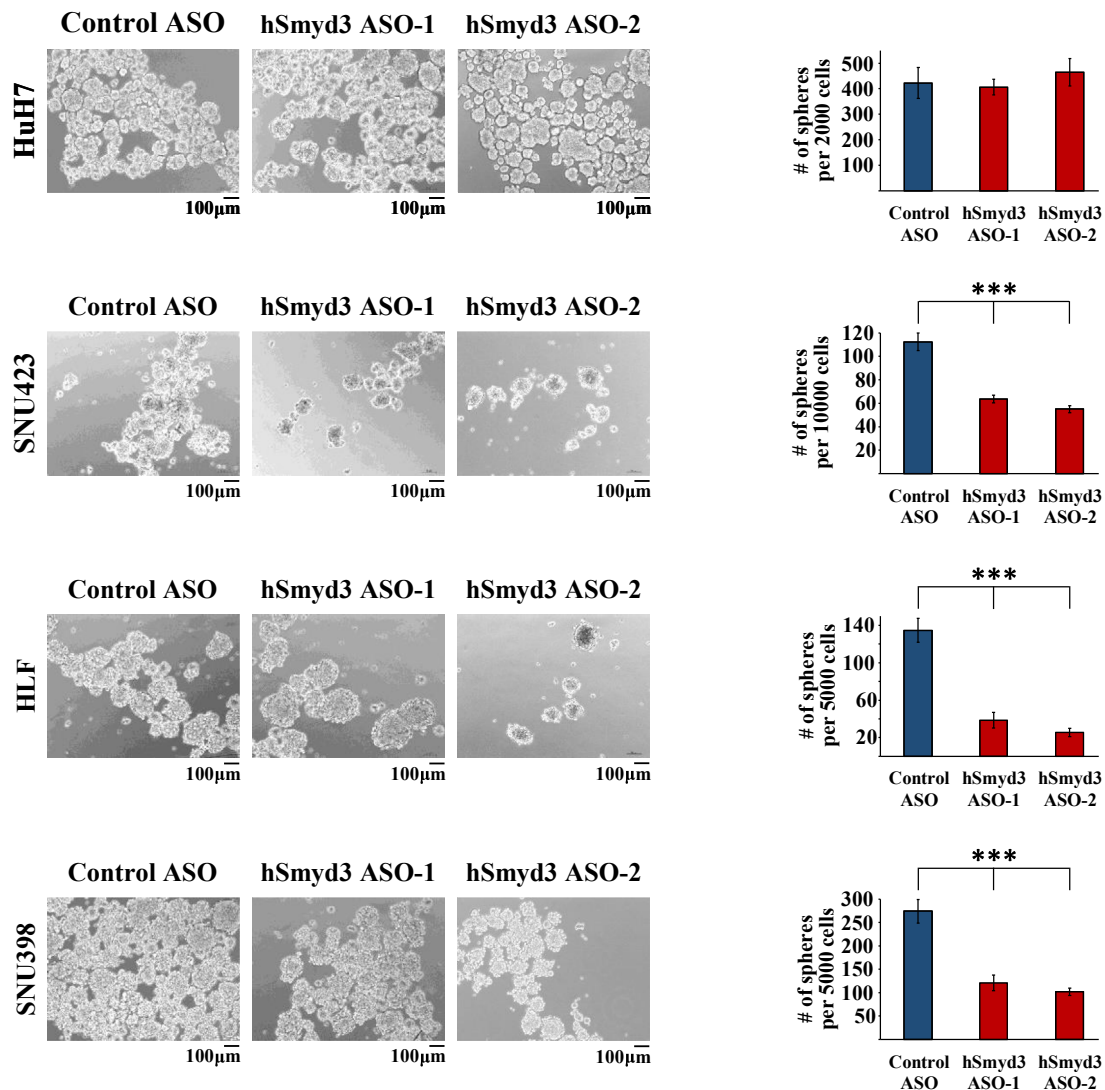
Figure 6. The effect of Smyd3-ASO treatment on oncosphere formation of human hepatocellular carcinoma cell lines

Representative images of oncospheres formed by 0.2 μM control-ASO and hSmyd3-ASO-1 or hSmyd3-ASO-2-treated HuH7, HLF, SNU398, SNU423, and SNU449 cells. Graphs at the right show quantitation of the average number of oncospheres (>70 μm diameter) formed at day 7 of culture in serum-free, growth factor supplemented medium and SEM from 4 independent experiments.

See also Figures S5, S6, and S8.

SNU449 cells pretreated with ASOs, the animals were treated twice weekly with hSmyd3-ASOs or control ASO. Among the cell lines of this study, only HuH7, HLF, and SNU398 gave rise to xenograft tumors. hSmyd3-ASO-1 treatment significantly reduced the size of xenograft tumors derived from HLF and SNU398-sensitive cells but not those derived from the resistant HuH7 cell line (Figure 7A), which is in line with the *in vitro* results of oncosphere formation (Figure 6) and growth or colony formation assays (Figures 5A and 5B). Since intraperitoneal administration of human Smyd3-ASOs specifically silenced Smyd3 expression of xenograft tumors (Figure 7A), we also tested their effect on the growth of already established xenograft tumors. As shown in Figure 7B, systemic administration of hSmyd3-ASOs targeting different regions of Smyd3 in mice, 10 days after the grafting of SNU398 cells, significantly delayed the growth of the already initiated xenograft tumors with concomitant reduction of Smyd3 mRNA levels.

Taken together, the above results demonstrate that hSmyd3-ASO-mediated silencing negatively influences the tumorigenic activity of human HCC-derived established cell lines.
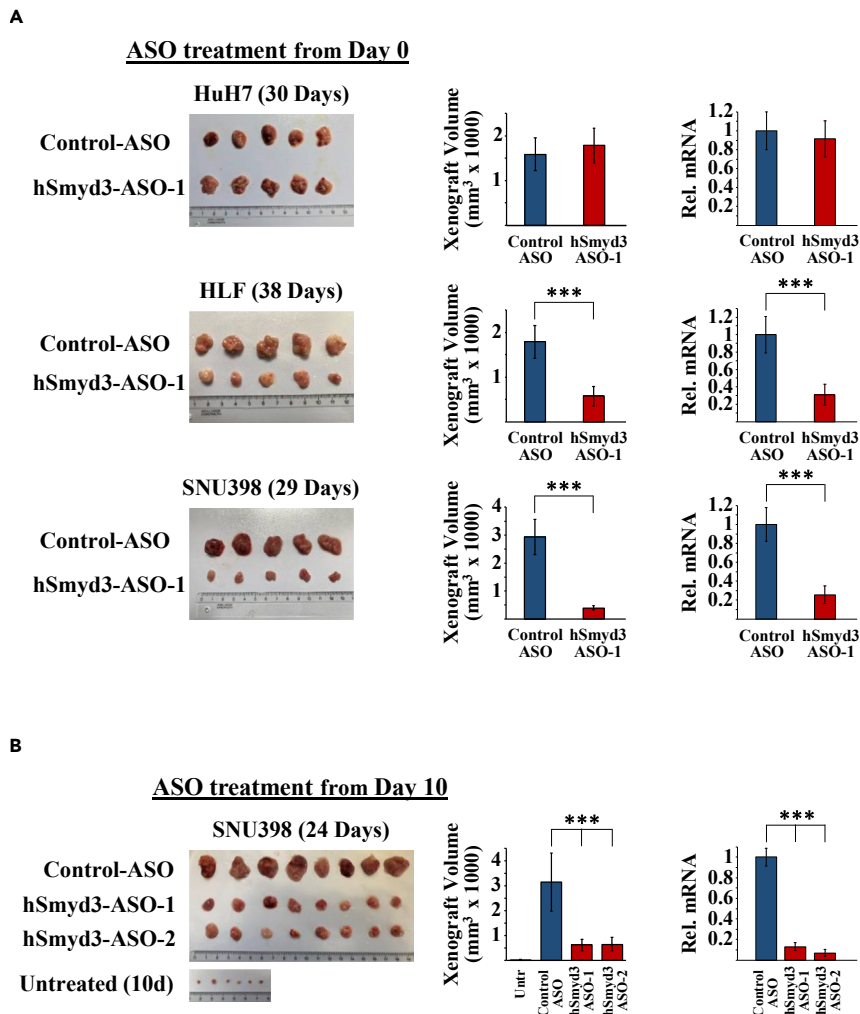
Figure 7. The effect of Smyd3-ASO treatment on xenograft formation of human hepatocellular carcinoma cell lines

(A) Pictures of subcutaneous xenograft tumors dissected from immunodeficient NSG mice at the indicated days following injection with HuH7, HLF, and SNU398 cells that were pretreated with 0.2 μM control-ASO or hSmyd3-ASO-1 for one passage. Following injection, the mice were treated intraperitoneally twice weekly with the ASOs at 50 mg/kg, as indicated. Graphs at the right show quantitation of the volumes of the xenografts. Bars represent average volumes of the 5 tumors and SEM.

(B) Picture of xenografts by untreated SNU398 cells 10 days after injection (bottom panel). The upper panel shows xenografts from mice that were treated with the indicated ASOs twice weekly from day 10 to day 24. Graphs at the right show quantitation of the volumes of the xenografts. Bars represent average volumes of the 8 tumors and SEM.

DISCUSSION

Systemic cancer therapies aim at targeting the specialized steps of the carcinogenic pathways to limit toxicity. Currently, the most efficient pharmacological agent for HCC treatment is sorafenib, which targets a broad array of tyrosine kinases and downstream pathways (Llovet et al., 2008). Most promising second- and third-line therapies under trials utilize similar broad specificity kinase inhibitors or checkpoint inhibitors, a form of immunotherapy (Likhitsup et al., 2019). Although combination of available strategies can be promising, the exploration of novel, highly specific targets is crucial to achieve improved therapeutic outcomes. Smyd3 has recently emerged as a highly promising target for the treatment of various cancer types, including HCC (Sarris et al., 2016; Giakountis et al., 2017; Mazur et al., 2014; Fenizia et al., 2019). Due to the requirement of high levels of Smyd3 for HCC development and its very low protein levels in physiological conditions, targeting Smyd3 offers unprecedented cancer specificity (Sarris et al., 2016; Giakountis et al., 2017).

During the past years, several molecular probes for Smyd3 have been developed (Fabini et al., 2019). A recent comprehensive study using a highly potent and specific enzymatic inhibitor of Smyd3, as well as genetic or siRNA-mediated inactivation of Smyd3 in a large panel of cell lines, failed to detect direct effects on cell growth (Thomenius et al., 2018). These results are in disagreement with *in vitro* data from others (Mazur et al., 2014; Peserico et al., 2015; Fenizia et al., 2019; Hamamoto et al., 2006; Bottino et al., 2020) or with data from mouse knockout studies and their correlation analyses with human HCC data, which demonstrated a definite onco-genic function of Smyd3 (Sarris et al., 2016; Mazur et al., 2014). Nevertheless, they raise the possibility that Smyd3-mediated regulation of cell proliferation may be more prominent in the *in vivo* organismal context. This scenario is also supported by the data of this study showing a strong effect of Smyd3 inhibition on the number of cells stained positive for the proliferation marker Ki67 in DEN-treated livers and the less dramatic influence on the growth of established hepatic cell lines. It is also possible that Smyd3-dependent regulation of other oncogenic pathways may have a greater contribution to the overall HCC phenotype, while prolifera-tion is affected as a secondary consequence of their activation. Such cancer-related processes requiring high Smyd3 levels are the activation of other oncogenes, the induction of epithelial-mesenchymal transition (EMT) (Sarris et al., 2016; Fenizia et al., 2019), and the promotion of cellular de-differentiation (Sarris et al., 2016).

Depending on cancer types, Smyd3-mediated oncogenic function is mediated through the methylation of histones (Peserico et al., 2015) or non-histone proteins (Mazur et al., 2014) or through potentiation of RNA Pol-II transcription (Sarris et al., 2016). The different requirements for the methylase activity of Smyd3 pro-vided the basis for searching intervention strategies that lower Smyd3 expression levels in tumors, as alter-native to the classical enzymatic inhibition approach.

In this study, we tested the efficacy of ASO-mediated pharmacological silencing of Smyd3 mRNA in already initiated DEN-induced liver tumors. We observed a dramatic inhibition of tumor development following mSmyd3-ASO treatment. Global gene expression profiling identified a distinct set of Smyd3-ASO-sensitive genes, whose differential expression specifies cellular de-differentiation processes, a hallmark feature of highly aggressive HCC and other types of cancers. Smyd3-ASO treatment prevented the cancer-depen-dent downregulation of genes characteristic of differentiated hepatocyte phenotypes and the activation of several key oncofetal genes. Differential expression of the Smyd3-ASO-sensitive de-differentiation-related gene cluster in patients with HCC correlated with the probability of tumor stage or tumor grade progression. Correlation with the more complex phenotype of OS probability was also significant, albeit only with a subgroup of the Smyd3-ASO-sensitive genes, which are negatively regulated during cancer development. Similar to Smyd3-KO mice (Sarris et al., 2016), several key genes of the cell proliferation, EMT, or oncogene activation pathways were also found affected in Smyd3-ASO-treated mice, a condition where Smyd3 is inhibited at a time subsequent to cancer initiation. However, the most prominent Smyd3-ASO-sensitive gene signature specifies cellular de-differentiation phenotypes.

De-differentiation processes in cancer are pivotal for the generation and expansion of CSCs, which play role in cancer cell renewal and metastatic potential and correlate with the level of aggressiveness and drug resistance of the tumor (Atashzar et al., 2020; Schulte et al., 2020; Nikolaou et al., 2015). Smyd3-ASO treatment prevented the overexpression of genes specifying hepatic CSC lineage like CD133, Sox9, Aldh, Dlk1, Sox9, Gpc3, Prom2, Sall1, Esm1, TFF3, Dusp1, Dntt, and Spp1, suggesting that the emer-gence or the expansion of the CSC population is suppressed by Smyd3 inhibition. This notion is further sup-ported by functional assays with established human hepatic cancer cell lines. While Smyd3-ASO treatment had small, albeit significant, effects on cell proliferation, more substantial changes were observed in assays related to stemness properties, like 3D oncosphere formation and *in vivo* xenograft growth.

Taken together, the above findings suggest that Smyd3-ASO treatment has the potential to prevent cellular de-differentiation and expansion of hepatic CSCs, a population that has been presumed to resist chemotherapy. Furthermore, the results provide preclinical evidence for the use of Smyd3-ASOs to treat already initiated HCC and warrant clinical studies investigating Smyd3-ASO therapy in patients.

Limitations of the study

Although our study clearly indicates that the tumor suppression effects are mainly mediated through silencing Smyd3 in hepatocytes, information about the role of Smyd3 expressed in other cell types of the liver cancer tissue (especially in inflammatory cells) is missing. Future single-cell transcriptomic analyses would clarify the role of Smyd3 in these cells.

STAR★METHODS

Detailed methods are provided in the online version of this paper and include the following:

- KEY RESOURCES TABLE
- RESOURCE AVAILABILITY
  - Lead contact
  - Materials availability
  - Data and code availability
- EXPERIMENTAL MODEL AND SUBJECT DETAILS
  - Mice and treatments
  - Cell lines
- METHOD DETAILS
  - Antisense oligonucleotides (ASOs)
  - H&E and immunostaining staining
  - ALT assays
  - RNA preparation and RT-PCR
  - Western blot analysis
  - RNA-sequencing and analyses
  - Differential expression analysis
  - Gene Set Enrichment Analysis
  - Comparative analyses using TCGA datasets
  - Growth curves
  - Colony formation assays
  - Oncosphere assay
  - Xenograft assay
  - Migration assay
- QUANTIFICATION AND STATISTICAL ANALYSIS

SUPPLEMENTAL INFORMATION

Supplemental information can be found online at https://doi.org/10.1016/j.isci.2021.102473.

AUTHOR CONTRIBUTIONS

H.K., Y.K., and I.T. conceived and designed the study. H.K., M.K., E.D., X.L., and I.T. performed experiments and evaluated data. M.V. and A.G. performed bioinformatics analyses. I.T. wrote the manuscript. All authors edited the text.

DECLARATION OF INTERESTS

Y.K. and X.L. are employees and shareholders of Ionis Pharmaceuticals. All other authors declare no potential conflicts of interest.

INCLUSION AND DIVERSITY STATEMENT

The author list of this paper includes contributors from the location where the research was conducted who participated in the data collection, design, analysis, and/or interpretation of the work.

REFERENCES

Anders, S., and Huber, W. (2010). Differential expression analysis for sequence count data. Genome Biol. *11*, R106.

Arun, G., Diermeier, S., Akerman, M., Chang, K.C., Wilkinson, J.E., Hearn, S., Kim, Y., MacLeod, A.R., Krainer, A.R., Norton, L., et al. (2016). Differentiation of mammary tumors and reduction in metastasis upon Malat1 lncRNA loss. Genes Dev. *30*, 34–51.

Atashzar, M.R., Baharlou, R., Karami, J., Abdollahi, H., Rezaei, R., Pourramezan, F., and Zoljalali Moghaddam, S.H. (2020). Cancer stem cells: a review from origin to therapeutic implications. J. Cell. Physiol. *235*, 790–803.

Bottino, C., Peserico, A., Simone, C., and Caretti, G. (2020). SMYD3: an oncogenic driver targeting epigenetic regulation and signaling pathways. Cancers (Basel) *12*, 142.

Cancer Genome Atlas Research Network. Electronic address, wheeler@bcm.edu, and Cancer Genome Atlas Research Network (2017). Comprehensive and integrative genomic characterization of hepatocellular carcinoma. Cell *169*, 1327–1341 e1323.

De Velasco, M.A., Kura, Y., Sakai, K., Hatanaka, Y., Davies, B.R., Campbell, H., Klein, S., Kim, Y., MacLeod, A.R., Sugimoto, K., et al. (2019). Targeting castration-resistant prostate cancer with androgen receptor antisense oligonucleotide therapy. JCI Insight *4*, e122688.

Di, Y., Schafer, D.W., Cumbie, J.S., and Chang, J.H. (2011). The NBP negative Binomial model for assessing differential gene expression from RNA-seq. Stat. Appl. Genet. Mol. Biol. *10*, 1–28.

Elkouris, M., Kontaki, H., Stavropoulos, A., Antonoglou, A., Nikolaou, K.C., Samiotaki, M., Szantai, E., Saviolaki, D., Brown, P.J., Sideras, P., et al. (2016). SET9-Mediated regulation of TGF-beta signaling links protein methylation to pulmonary fibrosis. Cell Rep. *15*, 2733–2744.

Fabini, E., Manoni, E., Ferroni, C., Rio, A.D., and Bartolini, M. (2019). Small-molecule inhibitors of lysine methyltransferases SMYD2 and SMYD3: current trends. Future Med. Chem. *11*, 901–921.

Fenizia, C., Bottino, C., Corbetta, S., Fittipaldi, R., Floris, P., Gaudenzi, G., Carra, S., Cotelli, F., Vitale, G., and Caretti, G. (2019). SMYD3 promotes the epithelial-mesenchymal transition in breast cancer. Nucleic Acids Res. *47*, 1278–1293.

Giakountis, A., Moulos, P., Sarris, M.E., Hatzis, P., and Talianidis, I. (2017). Smyd3-associated regulatory pathways in cancer. Semin. Cancer Biol. *42*, 70–80.

Hamamoto, R., Furukawa, Y., Morita, M., Iimura, Y., Silva, F.P., Li, M., Yagyu, R., and Nakamura, Y. (2004). SMYD3 encodes a histone methyltransferase involved in the proliferation of cancer cells. Nat. Cell Biol. *6*, 731–740.

Hamamoto, R., Silva, F.P., Tsuge, M., Nishidate, T., Katagiri, T., Nakamura, Y., and Furukawa, Y. (2006). Enhanced SMYD3 expression is essential for the growth of breast cancer cells. Cancer Sci. *97*, 113–118.

Hong, D., Kurzrock, R., Kim, Y., Woessner, R., Younes, A., Nemunaitis, J., Fowler, N., Zhou, T., Schmidt, J., Jo, M., et al. (2015). AZD9150, a next-generation antisense oligonucleotide inhibitor of STAT3 with early evidence of clinical activity in lymphoma and lung cancer. Sci. Transl. Med. *7*, 314ra185.

Karagianni, P., Moulos, P., Schmidt, D., Odom, D.T., and Talianidis, I. (2020). Bookmarking by non-pioneer transcription factors during liver development establishes competence for future gene activation. Cell Rep. *30*, 1319–1328.

Kim, D., Paggi, J.M., Park, C., Bennett, C., and Salzberg, S.L. (2019a). Graph-based genome alignment and genotyping with HISAT2 and HISAT-genotype. Nat. Biotechnol. *37*, 907–915.

Kim, Y., Jo, M., Schmidt, J., Luo, X., Prakash, T.P., Zhou, T., Klein, S., Xiao, X., Post, N., Yin, Z., and MacLeod, A.R. (2019b). Enhanced potency of GalNAc-conjugated antisense oligonucleotides in hepatocellular cancer models. Mol. Ther. *27*, 1547–1557.

Kole, R., Krainer, A.R., and Altman, S. (2012). RNA therapeutics: beyond RNA interference and antisense oligonucleotides. Nat. Rev. Drug Discov. *11*, 125–140.

Lawrence, M., Huber, W., Pages, H., Aboyoun, P., Carlson, M., Gentleman, R., Morgan, M.T., and Carey, V.J. (2013). Software for computing and annotating genomic ranges. PLoS Comput. Biol. *9*, e1003118.

Likhitsup, A., Razumilava, N., and Parikh, N.D. (2019). Treatment for advanced hepatocellular carcinoma: current standard and the future. Clin. Liver Dis. (Hoboken) *13*, 13–19.

Linnane, E., Davey, P., Zhang, P., Puri, S., Edbrooke, M., Chiarparin, E., Revenko, A.S., Macleod, A.R., Norman, J.C., and Ross, S.J. (2019). Differential uptake, kinetics and mechanisms of intracellular trafficking of next-generation antisense oligonucleotides across human cancer cell lines. Nucleic Acids Res. *47*, 4375–4392.

Llovet, J.M., Ricci, S., Mazzaferro, V., Hilgard, P., Gane, E., Blanc, J.F., de Oliveira, A.C., Santoro, A., Raoul, J.L., Forner, A., et al. (2008). Sorafenib in advanced hepatocellular carcinoma. N. Engl. J. Med. *359*, 378–390.

Love, M.I., Huber, W., and Anders, S. (2014). Moderated estimation of fold change and dispersion for RNA-seq data with DESeq2. Genome Biol. *15*, 550.

Maeda, S., Kamata, H., Luo, J.L., Leffert, H., and Karin, M. (2005). IKKbeta couples hepatocyte death to cytokine-driven compensatory proliferation that promotes chemical hepatocarcinogenesis. Cell *121*, 977–990.

Mazur, P.K., Reynoird, N., Khatri, P., Jansen, P.W., Wilkinson, A.W., Liu, S., Barbash, O., Van Aller, G.S., Huddleston, M., Dhanak, D., et al. (2014). SMYD3 links lysine methylation of MAP3K2 to Ras-driven cancer. Nature *510*, 283–287.

Morris, J.A., and Gardner, M.J. (1988). Calculating confidence intervals for relative risks (odds ratios)

and standardised ratios and rates. Br. Med. J. (Clin Res. Ed.) *296*, 1313–1316.

Moulos, P., and Hatzis, P. (2015). Systematic integration of RNA-Seq statistical algorithms for accurate detection of differential gene expression patterns. Nucleic Acids Res. *43*, e25.

Murray, S., Ittig, D., Koller, E., Berdeja, A., Chappell, A., Prakash, T.P., Norrbom, M., Swayze, E.E., Leumann, C.J., and Seth, P.P. (2012). TricycloDNA-modified oligo-2'-deoxyribonucleotides reduce scavenger receptor B1 mRNA in hepatic and extra-hepatic tissues–a comparative study of oligonucleotide length, design and chemistry. Nucleic Acids Res. *40*, 6135–6143.

Nikolaou, K.C., Moulos, P., Chalepakis, G., Hatzis, P., Oda, H., Reinberg, D., and Talianidis, I. (2015). Spontaneous development of hepatocellular carcinoma with cancer stem cell properties in PR-SET7-deficient livers. EMBO J. *34*, 430–447.

Nikolaou, K.C., Moulos, P., Harokopos, V., Chalepakis, G., and Talianidis, I. (2017). Kmt5a controls hepatic metabolic pathways by facilitating RNA Pol II release from promoter-proximal regions. Cell Rep. *20*, 909–922.

Pandit, H., Li, Y., Li, X., Zhang, W., Li, S., and Martin, R.C.G. (2018). Enrichment of cancer stem cells via beta-catenin contributing to the tumorigenesis of hepatocellular carcinoma. BMC Cancer *18*, 783.

Peserico, A., Germani, A., Sanese, P., Barbosa, A.J., Di Virgilio, V., Fittipaldi, R., Fabini, E., Bertucci, C., Varchi, G., Moyer, et al.. (2015). A SMYD3 small-molecule inhibitor impairing cancer cell growth. J. Cell. Physiol. *230*, 2447–2460.

Robinson, M.D., McCarthy, D.J., and Smyth, G.K. (2010). edgeR: a Bioconductor package for differential expression analysis of digital gene expression data. Bioinformatics *26*, 139–140.

Sarris, M., Nikolaou, K., and Talianidis, I. (2014). Context-specific regulation of cancer epigenomes by histone and transcription factor methylation. Oncogene *33*, 1207–1217.

Sarris, M.E., Moulos, P., Haroniti, A., Giakountis, A., and Talianidis, I. (2016). Smyd3 is a transcriptional potentiator of multiple cancer-promoting genes and required for liver and colon cancer development. Cancer Cell *29*, 354–366.

Schmieder, R., and Edwards, R. (2011). Quality control and preprocessing of metagenomic datasets. Bioinformatics *27*, 863–864.

Schulte, L.A., Lopez-Gil, J.C., Sainz, B., Jr., and Hermann, P.C. (2020). The cancer stem cell in hepatocellular carcinoma. Cancers (Basel) *12*, 684.

Seth, P.P., Siwkowski, A., Allerson, C.R., Vasquez, G., Lee, S., Prakash, T.P., Wancewicz, E.V., Witchell, D., and Swayze, E.E. (2009). Short antisense oligonucleotides with novel 2'-4' conformationaly restricted nucleoside analogues show improved potency without increased toxicity in animals. J. Med. Chem. *52*, 10–13.

Subramanian, A., Tamayo, P., Mootha, V.K., Mukherjee, S., Ebert, B.L., Gillette, M.A., Paulovich, A., Pomeroy, S.L., Golub, T.R., Lander, E.S., and Mesirov, J.P. (2005). Gene set enrichment analysis: a knowledge-based approach for interpreting genome-wide expression profiles. Proc. Natl. Acad. Sci. U S A *102*, 15545–15550.

Tarazona, S., Garcia-Alcalde, F., Dopazo, J., Ferrer, A., and Conesa, A. (2011). Differential expression in RNA-seq: a matter of depth. Genome Res. *21*, 2213–2223.

Thomenius, M.J., Totman, J., Harvey, D., Mitchell, L.H., Riera, T.V., Cosmopoulos, K., Grassian, A.R., Klaus, C., Foley, M., Admirand,

E.A., et al. (2018). Small molecule inhibitors and CRISPR/Cas9 mutagenesis demonstrate that SMYD2 and SMYD3 activity are dispensable for autonomous cancer cell proliferation. PLoS One *13*, e0197372..

Van Aller, G.S., Reynoird, N., Barbash, O., Huddleston, M., Liu, S., Zmoos, A.F., McDevitt, P., Sinnamon, R., Le, B., Mas, G., et al. (2012). Smyd3 regulates cancer cell phenotypes and catalyzes histone H4 lysine 5 methylation. Epigenetics *7*, 340–343.

Ward Rashidi, M.R., Mehta, P., Bregenzer, M., Raghavan, S., Fleck, E.M., Horst, E.N., Harissa, Z., Ravikumar, V., Brady, S., Bild, A., et al. (2019). Engineered 3D model of cancer stem cell

enrichment and chemoresistance. Neoplasia *21*, 822–836.

Xiao, L., Tien, J.C., Vo, J., Tan, M., Parolia, A., Zhang, Y., Wang, L., Qiao, Y., Shukla, S., Wang, X., et al. (2018). Epigenetic reprogramming with antisense oligonucleotides enhances the effectiveness of androgen receptor inhibition in castration-resistant prostate cancer. Cancer Res. *78*, 5731–5740.

Xu, S., Zhou, T., Doh, H.M., Trinh, K.R., Catapang, A., Lee, J.T., Braas, D., Bayley, N.A., Yamada, R.E., Vasuthasawat, A., et al. (2019). An HK2 antisense oligonucleotide induces Synthetic lethality in HK1(-)HK2(+) multiple myeloma. Cancer Res. *79*, 2748–2760.

STAR★METHODS

KEY RESOURCES TABLE

REAGENTS or RESOURCES	SOURCE	IDENTIFIER
Antibodies		
Anti-P-H2A.X	Cell Signaling Technology	#9718
Anti-Smyd3	Sarris et al., 2016	
GAPDH antibody (6C5)	Santa Cruz Biotechnology	sc-32233
Anti-rabbit IgG, HRP-linked antibody	Cell Signaling Technology	#7074
Goat anti-rabbit IgG (H + L) Alexa Fluor 568	Thermo Fisher	A-1011
Chemicals, peptides, and recombinant proteins		
Complete, EDTA-free protease inhibitor cocktail	Roche	11873580001
Proteinase K	Thermo Scientific	17916
Formaldehyde (37% solution)	AppliChem	A0877,0250
Diethylnitrosamine	Sigma	N0756
NucleoZOL	Macherey-Nagel	740404.200
Trizol reagent	Life Technologies	15,596-026
MMLV reverse transcriptase	Promega	M1701
DNaseI recombinant, RNase-free	Roche	04716728001
FastStart Universal SYBR Green Master	Roche	10689400
Tissue-Tek O.C.T. Compound	Sakura	4583
Papanicolaou's solution 1a Harris' hematoxylin	Sigma	1092530500
Eosin Y	Sigma	230251
Oligo(dT)12-18	Thermo Fisher	18418012
Dulbecco's modified Eagle medium	Thermo Fisher	41965039
Fetal bovine serum	Thermo Fisher	26140079
BSA fraction IV fatty acid free	Sigma-Aldrich	05,482
ProLong gold antifade reagent with DAPI	Cell Signaling Technology	8961S
Crystal violet	Sigma	C0775
Recombinant mouse FGF-basic	PeproTech	450-33
Recombinant mouse EGF	PeproTech	315-09
N-2 supplement (100x)	Thermo Fisher	17502048
B-27 supplement (50x) serum free	Thermo Fisher	17504044
Methylcellulose	Sigma	M7027
BD matrigel matrix growth factor reduced	BD Biosciences	365234
Critical commercial assays		
ALT assay kit	DiaSys	127019910021
QuantSeq 3′ mRNA-Seq FWD	Lexogen	015.24/96/2×96
Agencourt AMPure XP	Beckman Coulter	A63881
SuperSignal West Pico PLUS chemiluminescent Substrate	Thermo Fisher	34,580
Deposited data		
RNA-seq data	This paper	GSE150377
TCGA level 3 LIHC data set	Cancer Genome Atlas Research Network et al., 2017	N/A

(Continued on next page)

Continued

REAGENTS or RESOURCES	SOURCE	IDENTIFIER
Experimental models: cell lines		
SNU387	American Type Culture Collection (ATCC)	CRL-2237
SNU398	American Type Culture Collection (ATCC)	CRL-2233
SNU423	American Type Culture Collection (ATCC)	CRL-2238
SNU449	American Type Culture Collection (ATCC)	CRL-2234
HuH7	Japanese Cancer Research Cell Bank	JCRB0403
HLF	Japanese Cancer Research Cell Bank	JCRB0405
Experimental models: organisms/strains		
C57Bl/6 mouse	Jackson Laboratory	N/A
Balb/cJ mouse	Jackson Laboratory	N/A
NOD.Cg-Prkdc^{scid} Il2rg^{tm1Wjl} /SzJ	Jackson Laboratory	N/A
Oligonucleotides		
mSmyd3 forward primer, 5′-TGC TGA TGA CCA GCG AGG AAC G 3′	Thermo Fisher	NM_027188.3
mSmyd3 Reverse primer, 5′ AAC CTG CTC CCA CTT CCA GTG C 3′	Thermo Fisher	NM_027188.3
mGAPDH Forward primer, 5′ CCA ATG TGT CCG TCG TGG ATC T 3′	Thermo Fisher	NM_008084
mGAPDH Reverse primer, 5′ GTT GAA GTC GCA GGA GAC AAC C 3′	Thermo Fisher	NM_008084
hSmyd3 Forward primer, 5′ CAA ACT GCA GCT ACA TCA AGG 3′	Thermo Fisher	NM_001167740.2
hSmyd3 Reverse primer, 5′ TCT CTG CCA TGT GTC ACT C 3′	Thermo Fisher	NM_001167740.2
hGAPDH Forward primer, 5′-CAT GTT CCA ATA TGA TTC CAC C-3′	Thermo Fisher	NM_001256799.3
hGAPDH Reverse primer, 5′-GAT GGG ATT TCC ATT GAT GAC-3′	Thermo Fisher	NM_001256799.3
Software and algorithms		
PRINSEQ version 0.20.4	Schmieder and Edwards, 2011	N/A
DESeq2	Anders and Huber, 2010	N/A
FastQC	https://www.bioinformatics.babraham.ac.uk/projects/fastqc/	N/A
edgeR	Robinson et al., 2010	N/A
NOISeq	Tarazona et al., 2011	N/A
Limma	www.bioconductor.org/packages/devel/bioc/vignettes/limma/inst/doc/	N/A
metaseqR	Moulos and Hatzis, 2015	N/A

RESOURCE AVAILABILITY

Lead contact

Further information and requests for reagents may be directed to and will be fulfilled by the lead contact Iannis Talianidis (talianid@imbb.forth.gr)

Materials availability

Unique reagents of this study are next-generation antisense oligonucleotides, which will be made available for research purposes after completion of Material Transfer Agreement with Ionis Pharmaceuticals.

Data and code availability

RNA sequence data of this study have been deposited at GEO data base under accession number: GSE150377.

EXPERIMENTAL MODEL AND SUBJECT DETAILS

Mice and treatments

C57Bl/6J (Jackson Laboratory), BALB/c and NSG (NOD.Cg-Prkdc^{scid} Il2rg^{tm1Wjl} /SzJ) mice were maintained in grouped cages in a temperature-controlled, pathogen-free facility on a 12 hr light/dark cycle and fed a standard chow diet containing 19% protein and 5% fat (Altromin 1324) and water ad libitum. All animal experiments were approved by the Ethical Review Board of IMBB-FORTH and the Animal Ethics Committee of the Prefecture of Crete and were performed in accordance with the respective national and European Union regulations. All experiments were performed in randomly chosen age-matched male mice. No blinding was used in this study. Liver tumors were induced by a single intraperitoneal injection of 25 mg/kg diethylnitrosamine (DEN, N0756; Sigma) at postnatal day 14. ASO treatments were performed by intraperitoneal injections, twice weekly following postnatal day 133 (P133). Mice were sacrificed at P133 or P260. Lethality rate in control ASO and Smyd3-ASO treated mice was 1 out of 10 during the P260 experimental period. In short-term treatments, mice were injected twice weekly for 4 weeks, with the first injection at day 1 of the program and last injection at the day before the sacrifice.

Cell lines

The human HCC cell lines SNU387 (from grade IV/V pleomorphic HCC), SNU398, SNU423 (from grade III/IV pleomorphic HCC) and SNU449 (from grade II-IV HCC) were from ATCC, HuH7 and HLF cells were from Japanese Cancer Research Foundation (JCRF).

METHOD DETAILS

Antisense oligonucleotides (ASOs)

Next-generation (Gen 2.5) ASOs with constrained ethyl (cEt) modification on the sugar were synthesized as described previously (Seth et al., 2009). The ASOs used in the study were selected as follows: Approximately, 300 ASOs covering the entire transcript of Smyd3 were designed. Their potencies were first tested in A431 cells at 0.2 μM for human ASOs and in Hepa1-6 cells at 1 μM for mouse ASOs, which was followed by 5 points dose response experiments with ~40 ASOs. Among them, top 15 ASOs were selected for in vivo tolerability studies where male Balb/c mice at 4-6 weeks of age (n=4/group) were treated subcutaneously with the ASOs prepared in PBS, twice a week at 50 mg/kg for 4 weeks. At the end of the study, changes in organ weights (liver, kidney, and spleen) and blood chemistry (ALT, AST, BUN, Albumin, T.Bil) were measured. The top 2 to 3 ASOs with minimal elevations in those parameters were selected for further in vitro and in vivo studies. In the case of mouse Smyd3 ASOs, Smyd3 mRNA levels were measured in liver and colon at the end of 4-week tolerability study. A negative control ASO with no perfect match to any genes in the genome was included in each study to rule out any potential non-specific effects of ASO on changes in gene expression or phenotypes. The antisense oligonucleotides used in this study had the following sequences with underlined letters indicating cEt-modified bases:

Control ASO: 5' <u>CGC</u>CGATAAGGTA<u>CAC</u> 3'

Mouse Smyd3 ASO-1: 5' <u>GTA</u>TAAAGTTAGA<u>GCC</u> 3'

Mouse Smyd3 ASO-2: 5' <u>AAC</u>ATCTTACCAA<u>TGG</u> 3'

Human Smyd3 ASO-1: 5' <u>CGT</u>ATTAACACTGG<u>CA</u> 3'

Human Smyd3 ASO-2: 5' <u>TTT</u>AGTAGGTGCC<u>TCG</u> 3'

H&E and immunostaining staining

Liver tissue was fixed in 4% Formaldehyde/PBS overnight, followed by tissue dehydration and paraffin infiltration. The paraffin infiltrated liver tissues were embedded into wax blocks and sectioned using a Leica RM2255 microtome. Sections were deparaffinized with xylene and rehydrated by passing through series of graded ethanol (100%, 90%, 70%, 50%) for 3 min each. The slides were incubated in Papanicolaou's solution 1a Harris hematoxylin for 3 minutes and after extensive washings with tap water, were differentiated in 0.2% HCl, 70% ethanol for 3 minutes and washed again with water. The sections were incubated with 1% Eosin-Y for 3 minutes. After washing with water and dehydration in a series of graded ethanol (50%, 70%, 90%, 100%) the sections were mounted and observed with light microscopy.

Immunofluorescence staining was performed as described (Nikolaou et al., 2017; Elkouris et al., 2016). Briefly, freshly isolated liver tissues were embedded in Optimal Cutting Temperature (OCT) embedding medium and were frozen in liquid nitrogen. Frozen sections (5 μm thick) were fixed in 4% formaldehyde, blocked in 1% BSA/0,1% Triton X-100 for 1 hr and then incubated with anti-P-H2A.X antibody (Cell Signaling, #9718) at 4^0C overnight. After incubation with AlexaFluor 568-conjugated goat anti-rabbit secondary antibody for 1 hr at room temperature and counterstaining with DAPI, fluorescence images were observed using a Leica TCS Sp8 confocal microscope.

ALT assays

Blood was collected from the orbital sinus into heparinized polypropylene tubes. Following centrifugation at 1500 g for 15 minutes, cell-free plasma supernatant was taken for colorimetric ALT activity measurements using Dyasis ALAT (GPT) FS kit. The ALT enzymatic reaction product pyruvate was monitored by measuring its conversion by oxidation into a colored probe, detectable at OD260 as described (Nikolaou et al., 2015). Standard curves were established by measuring serial dilutions of pyruvate standard.

RNA preparation and RT-PCR

Total RNA was prepared from cell pellets or liver pieces (whole lobes) by homogenization in 10 volumes of Nucleozol reagent (Macherey-Nagel), followed by the addition of 2 volumes of chloroform and centrifugation at 12.000 g for 15 minutes. The aqueous phases were precipitated with isopropanol and subjected to a second extraction as above, but with Trizol reagent (Thermo Fisher Scientific). The RNA samples were digested with 10 units of DNase I for 10 min at $37\ ^0$C, extracted with phenol/chloroform and precipitated by ethanol.

For RT-PCR analysis, first strand cDNA synthesis was performed by incubating 1 μg of total RNA with 200 units of MMLV reverse transcriptase and 100 ng oligodT primer in a buffer containing 50 mM Tris-HCl pH 8.3, 75 mM KCl, 3 mM $MgCl_2$, 10 mM DTT for 60 minutes at $37\ ^0$C. Quantitative PCR analyses were carried out in STEP-ONE Real time PCR detection system using Fast Start Universal SYBR Green Master Mix and human or mouse Smyd3-specific oligonucleotide primers. The sequences of the primers are presented in Key Resource Table.

Western blot analysis

Cells were collected from the plates and washed 3 times with PBS, followed by lysis in 10 volumes of modified RIPA buffer containing 50 mM Tris (pH 7.5), 1% NP40, 0.25% Na-Deoxycholate, 150 mM NaCl, 1mM EDTA, 10% Glycerol, 1 mM NaF and protease inhibitors cocktail (Roche). After 20 min. incubation at 4 °C, extracted proteins were recovered by centrifugation at 14000 rpm. The extracts were resolved by 10% SDS-PAGE, transferred to Protran Nitrocellulose membrane. Following transfer, the membranes were washed with TBST (10 mM Tris (pH 8.0), 150 mM NaCl and 0.1% Tween 20) and blocked in TBST buffer containing 5% low-fat dry milk for 1 hour at room temperature. After washing with TBST, the membranes were stained with Smyd3 antibody (1:1000 dilution) in TBST-1% milk overnight at 4 °C. The membranes were washed with TBST and stained with the HRP-conjugated anti rabbit IgG secondary antibody for 1 hour at room temperature.

The filters were probed with Enhanced Chemiluminescent HRP substrate (ThermoFisher) and detected using ChemiDoc MP imaging system (BioRad).

RNA-sequencing and analyses

RNA-seq libraries were generated using QuantSeq 3' mRNA-Seq FWD kit from Lexogen and sequenced in an Illumina NextSeq 500 system. Raw sequence data were quality assessed and pre-processed using PRINSEQ version 0.20.4 (Schmieder and Edwards, 2011). More precisely, we removed all reads with mean Phred quality scores of less than 25 with the argument '-min_qual_mean 20'. Sequences were trimmed from both ends using a Phred quality score threshold of 20, using the options '-trim_qual_right 20' and '-trim_qual_left 20'. Finally, after the trimming operations, any sequence shorter than 60 bp was discarded using the argument '-min_len 60'. Pairs of samples that were technical replicates were merged into single representations and the pre-processed FASTQ files were subsequently mapped on the UCSC mm10 reference genome, using HISAT2 version 2.1.0 () with the argument –score-min L,0.0–0.5, setting the function for the minimum valid alignment score. The resulting BAM files were analyzed with the

Bioconductor package metaseqR (Moulos and Hatzis, 2015), which has built-in support for QuantSeq data. Briefly, the raw BAM files were summarized to a 3'UTR read counts table, using the Bioconductor package GenomicRanges (Lawrence et al., 2013). The final gene counts table for each gene model was calculated from the corresponding 3' UTR regions, where each row represented an Ensembl gene model and each column corresponded to a sample. Prior to any statistical testing, principal components analysis (PCA) and sample correlation analysis was performed to explore global read count patterns. For this analysis, the raw gene counts table was filtered removing features that had zero counts across all the samples and transformed with DESeq2 regularized-logarithm transformation (rlog) (Love et al., 2014). This function returns values that are both normalized for sequencing depth and transformed to the log2 scale in a way which minimizes the variance of low read counts. In order to assess the overall similarity between the Smyd3 ASO-1 and Smyd3 ASO-2 replicates, we created scatterplots of the rlog transformed counts and calculated the Pearson correlation coefficient between each pair.

Differential expression analysis

The raw gene counts table was normalized for inherent systematic or experimental biases using the Bioconductor package DESeq (Anders and Huber, 2010), after removing genes that had zero counts over all the samples. Prior to the statistical testing procedure, the gene read counts were filtered for possible artifacts that could affect the subsequent statistical testing procedures. Genes presenting any of the following were excluded from further analysis: i) genes with length less than 500bp, ii) genes with read counts below the median read counts of the total normalized count distribution, iii) genes whose biotype matched the following: rRNA, IG_V_pseudogene and TR_V_pseudogene, iv) genes where 25% of samples were not above 10 counts across all samples and v) genes with mean RPGM normalized values below 0.01 (i.e. the ratio of normalized reads per gene model). The resulting gene counts table was subjected to differential expression analysis for the appropriate contrasts using the Bioconductor packages DESeq (Love et al., 2014), edgeR (Robinson et al., 2010), NOISeq (Tarazona et al., 2011), limma (www.bioconductor.org/packages/devel/bioc/vignettes/limma/inst/doc/), NBPSeq (Di et al., 2011). In order to combine the statistical significance from multiple algorithms and perform meta-analysis, the PANDORA weighted p value method was applied. Genes presenting a Benjamini-Hochberg false discovery rate (FDR) less than 0.05 and fold change (for each contrast) greater than 0.58 or less than −0.58 in log2 scale corresponding to 1.5 times up and down in natural scale respectively were considered differentially expressed.

Gene Set Enrichment Analysis

For functional analysis of the genes, Gene Set Enrichment Analysis (GSEA) was performed with the C5 and C6 gene sets from the MSigDB (http://www.broadinstitute.org/gsea/msigdb) using the GSEA software version 3.0 (Subramanian et al., 2005) with default parameters and FDR<0.25 cutoff. The analysis was performed on the RPGM normalized expression values of the 'ASO sensitive' differentially expressed genes. The statistical significance (nominal p value) for the enrichment score (ES) was estimated by using a gene set permutation procedure of 1000 permutations.

Comparative analyses using TCGA datasets

The Human Cancer Genome Atlas (TCGA) RNA-seq and clinical data (Level 3 LIHC dataset) (Cancer Genome Atlas Research Network et al., 2017) were obtained from UCSC Xena. Preparation and filtering of RPKM values was performed as described (Sarris et al., 2016). For Figures 4A and 4B, gene ranking was performed with PCA in Perseus, based on normal vs tumor expression. More specifically, PCA was performed on the LIHC dataset after filtering the low expressed genes. Component 1 discriminated normal from tumor samples based on global gene expression and thus gene loadings of PC1 were used as ranking criterion. Low ranks (close to zero), corresponding to positive PC1 values, represent higher gene expression in tumors compared to normal biopsies. For Figures 4C and 4D survival analysis, Overall Survival (OS) Kaplan Meier analysis together with associated Log Rank p value calculation, was performed with R package Survminer for each expressed gene. Effect on survival for each individual gene was scored as "High" or "Low" if higher or lower expression (compared to expression median of each gene across all LIHC patients), corresponded to statistically significant shortening of survival time (Log Rank <0.05). Gene effect was scored as "None" if there was no statistical effect of gene expression of survival time. Since Survminer analysis is limited only to OS, for tumor grade or stage analysis (Figures 4E and 4F), ODDs ratio was used to relate individual gene expression with the probability of a significant clinical effect. For each expressed gene, a 2x2 contingency table was prepared based on the following criteria: for gene expression scoring (contingency table row criteria) "High" represents higher gene expression than tumor median across tumor

biopsies, "Low" represents lower expression than tumor median. For Stage scoring (contingency table column criteria) "1" represents patient samples at Stages III or IV, "0" represents patient samples at Stages I or II. For Grade scoring, "1" represents patient samples at grades G3 or 4, "0" represents patient samples at G1 or 2. ODDs ratio (OR) was calculated as described (Morris and Gardner, 1988). Next, all expressed genes (includes protein coding, pseudogenes and lncRNAs) were ranked based on their individual OR values for each clinical analysis (grade or stage) separately. Low ranks (close to zero) correspond to individual gene OR value > 1 and indicate that high expression increases the odds of progressed tumor stage or undifferentiated tumor grade. Kaplan Meyer Analyses for Tumor Stage and Tumor Grade correlation was performed by SigmaStat software.

Growth curves

The cells were maintained in Dulbecco's modified Eagle medium (DMEM) supplemented with 10% heat-inactivated fetal calf serum. For proliferation assays, the cells were treated with Smyd3-ASOs or Control ASO for one passage and seeded at 30% confluence. The medium was replaced with fresh ASO-containing media every 24 hr. At specific time points the plates were fixed with 4% formaldehyde and stained with DAPI. Cell numbers were counted using an Operetta (PerkinElmer) high content microscope and the data were evaluated using the Harmony Software 4.1 of PerkinElmer.

Colony formation assays

For colony formation assays 1000 cells were seeded onto 100 mm plates and cultured for 18-22 days. The medium was replaced with fresh ASO-containing media every other day. To visualize the colonies, the plates were fixed and stained with 0.5% crystal violet in absolute methanol for 5 min and washed extensively with distilled water. Colony numbers in each plate were counted using ImageJ software.

Oncosphere assay

Cell lines were trypsinized and dissociated into single cells. 2 to 10.000 cells were suspended in oncosphere media containing Advanced DMEM/F-12 supplemented with B-27 and N2 supplement, 20 ng/mL mouse EGF, 10 ng/mL mouse FGF-basic, 2 mM Glutamine, 100 μg/mL Penicillin, 100 U/ml streptomycin and 1% methylcellulose. Cells were plated in 24-well ultra-low attachment culture plates (Corning) and spheres with >70 μm diameter, were counted after 7 days. Five independent wells were used per cell line per experiment.

Xenograft assay

Cells were grown untreated or treated with ASOs *in vitro* for one passage. Following collection by trypsin digestion, 10^6 cells were washed with DMEM-10% FBS, mixed with equal volume BD-Matrigel and injected subcutaneously into the right or left flank of 2 months old NSG (NOD.Cg-Prkdc^{scid} Il2rg^{tm1Wjl} /SzJ) mice. The mice were treated with ASOs twice weekly. Subcutaneous tumors were isolated and their volumes were calculated by the formula V=1/2[(length).^2 x width].

Migration assay

10^5 cells resuspended in serum free DMEM were added to the top of 24-well Millicell hanging inserts (Millipore). As a chemoattractant, 0.75 ml DMEM-10% FBS was added to the bottom chamber. After 24 hours of incubation at 37^0C, cells that migrated or invaded through the membrane (migration) were fixed with 70% ethanol and stained with 0.2% crystal violet in 2% ethanol for 10 min. The inserts were washed extensively with distilled water and air-dried. The number of migrated cells were measured using ImageJ software.

QUANTIFICATION AND STATISTICAL ANALYSIS

Comparisons between two groups were performed using Student unpaired t test. All statistical analyses were performed with Graphpad Prism 7 and 8 (GraphPad). Error bars show SEM, as indicated in the legends, and $P < 0.05$ was considered statistically significant. (* indicates $p < 0.05$; **, $p < 0.01$; ***, $p < 0.001$; ns, not significant).